Pn growth on the (111) surface of the 1/1 Au-Al-Tb approximant: influence of surface geometry on adsorption

Sam Coates
Department of Materials Science and Technology, Tokyo University of Science, 6 Chome–3–1 Niijuku, Katsushika City, Tokyo 125-8585

Ronan McGrath and Hem Raj Sharma
Surface Science Research Centre and Department of Physics, University of Liverpool, Liverpool, L69 3BX, UK

Ryuji Tamura
Department of Materials Science and Technology, Tokyo University of Science, 6 Chome–3–1 Niijuku, Katsushika City, Tokyo 125-8585

Molecular adsorption on both quasicrystalline and approximant substrates has produced a number of pseudomorphic films, and has led to a deeper understanding of the chemistry of the surfaces of these materials. Here, the recently reported reconstructed (111) surface of the 1/1 Au–Al–Tb Tsai–type approximant has been used as a template for pentacene (Pn) adsorption, which is investigated using Scanning Tunnelling Microscopy (STM). This surface provides unique varieties of adsorption sites compared to normal metal surface. After room temperature deposition, the Pn molecules are mobile yet exhibit a structure which indicates a bond with the Tb atoms of the surface, while reflecting the 2–fold symmetrical nature of the reported Au/Al row reconstruction. Post–deposition annealing shows a linearised film of molecules which appears dependent on the relationship of the Tb atoms to the row structure.

I. INTRODUCTION

The wide compositional variety in Tsai–type quasicrystals and approximants has led to the observation of a range of phase–specific and stoichiometric–specific properties[1–6], including a rich array of magnetic transitions[7–12]. The shared building block of these materials, the Tsai–type cluster, is a hierarchical polyhedral structure consisting of 5 atomic shells: a tetrahedron, dodecahedron, icosahedron, icosidodecahedron and rhombic triacontahedron[13–15]. These polyhedra and their nested nature are indicated in Figure 1(a) by the black arrows, where the 1st shell is grey, 2nd is yellow, 3rd is green, 4th is blue, and 5th is red. The exact structural solution of Tsai–type materials gives license for a deep understanding of their properties, and, allows for informed analyses of their surfaces.

In general, the surfaces of quasicrystal approximants offer a diverse field of investigation, as their structural and chemical behaviour can be dissimilar to their quasicrystalline analogues, despite their common building blocks (not exclusive to Tsai–types). For instance, reconstructions (not seen in quasicrystals) and high surface corrugations indicate a potential for catalytic activity[16–18], while the periodicity of approximant surfaces offer different, yet novel, energetic landscapes for adsorbates[19–21].

We recently showed that the (111) surface of the anti–ferromagnetic 1/1 $Au_{70}Al_{16}Tb_{14}$ Tsai–type approximant forms a partial reconstruction[22] – the first reconstruction observed at a Tsai–type approximant surface[23,24]. Here the Au/Al atoms create a row–type structure, while the Tb atoms conform to the expected bulk truncation: small triangles in two 60°–related orientations and larger triangles in a singular orientation. A model of this surface structure is shown in Figure 1(b) where the atoms of specific shells are coloured according to Figure 1(a), and the Tb triangles are contained within black lines. This juxtaposition of 2–fold (Au/Al) and 3–fold (Tb) symmetry presents an intriguing playground

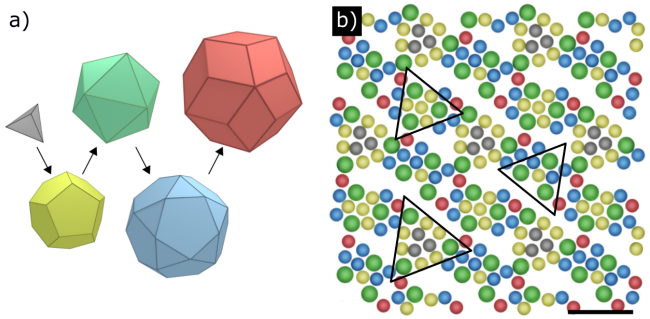

FIG. 1: **(a)** The hierarchical Tsai–cluster model. **(b)** Model of the (111) surface of the 1/1 Au–Al–Tb approximant. Green circles correspond to Tb atoms, the remaining colours are a stoichiometric mix of Au/Al. Scale bar is 1.5 nm.

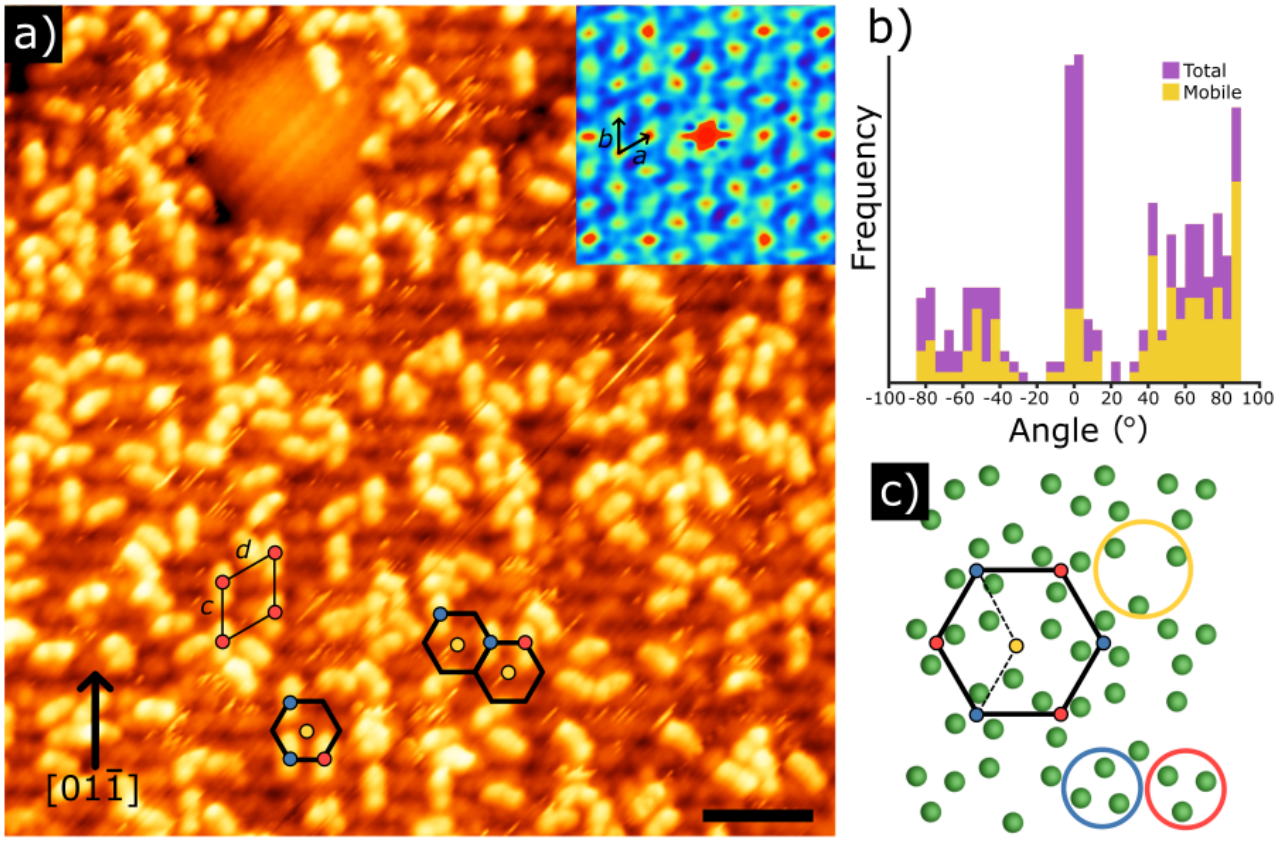

FIG. 2: **(a)** STM image (V_b = -1900 mV, I_t = 300 pA)) of the Au–Al–Tb(111) surface after deposition of 0.3 ML of Pn. Highlighted by red and blue circles are molecules which are both oriented along the same direction yet occupy distinctly different adsorption sites. These molecules occupy a honeycomb lattice, as marked by a black hexagon. Yellow circles indicate vacant positions. Inset is an autocorrelation function of the molecule centres, with unit cell vectors marked. The [01$\bar{1}$] direction is indicated by a black arrow. Scale bar is 5 nm. **(b)** A histogram of molecular orientations. Orange bars represent the total number of orientations, yellow bars represent the ratio of molecules which are observed diffusing. **(c)** A model of the Tb atoms at the surface. Blue and red circles indicate small Tb triangles which form a hexagonal unit cell, as marked in black. A larger yellow circle indicates a subsurface triangle. Small red, blue, and yellow dots sit at the centre of these triangles, replicating the motif in **(a)**. A dashed line indicates the cell formed by red, blue, and yellow triangles.

for adsorption studies.

Here, we present the deposition of pentacene (Pn) molecules onto the (111) surface of the 1/1 Au–Al–Tb approximant. There have been many previous surface studies utilizing pentacene as a model linear organic molecular adsorbate. In such studies, establishing the molecular adsorption geometry typically reveals useful knowledge about the underlying surface structure and reactivity. The molecule acts as a chemical probe of the surface, while also yielding using information on the role of intermolecular interactions in ordering processes on complex surfaces[26,27]. Here, at low coverage the Pn molecules are relatively mobile but are shown to adsorb at specific Tb sites. The observed orientational anisotropy of the adsorbed molecules indicates that there are certain preferred sites. Post–annealing of higher coverages reveals a linear Pn structure which appears related to the reconstructed Au/Al rows of the substrate.

II. METHODS

The (111) surface of a single crystal of 1/1 Au–Al–Tb was polished with successively finer grades of diamond paste (6–0.25 μm) before washing in methanol. The surface was then further cleaned with sputter–anneal cycles (30 minute Ar^+ sputter, 2 hour anneal at 730 K) under ultra–high vacuum conditions. Substrate cleanliness was monitored with room temperature scanning tunnelling microscopy (STM), where STM bias is given with respect to the tip. Pn was dosed using a homemade evaporator. Due to the location of the evaporator, the molecules were deposited on the sample held at room temperature, before post–dose annealing. The specifics of the molecular annealing temperatures and times are discussed later.

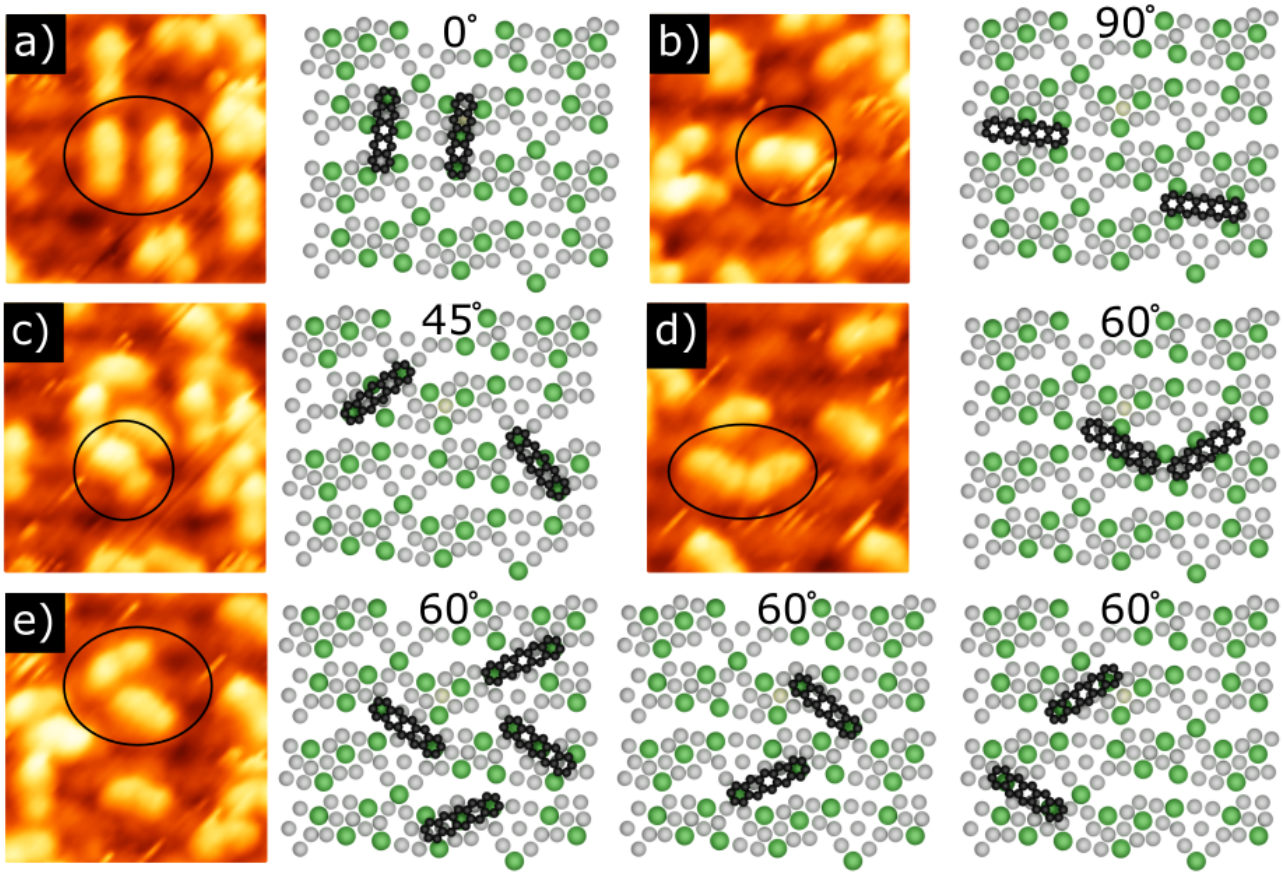

FIG. 3: (a–e) Enlarged STM images from Figure 2(a) and model representations of Pn adsorption sites for a range of Pn orientations. The relevant molecules are circled in black. In each case, the Pn molecule is either adsorbing directly on–top multiple Tb atoms (e.g. **(c)**, **(e)** middle and right), pinned by closely separated Tb atoms (**(b)**, **(d)**) or a mixture of both (remaining).

III. RESULTS AND DISCUSSION

Figure 2(a) shows an STM image of approximately 0.3 monolayers (ML) of Pn on the Au–Al–Tb(111) surface, estimated by removing the substrate contribution to the image area. In this case, 1 ML refers to complete areal coverage of the scan with molecules; the approximate number of molecules deposited was 0.11 per nm^2. The sample was held at room temperature during deposition, after which it was annealed at $\sim$ 370K for 10 minutes. The Pn molecules appear to sparsely decorate a rhombohedral lattice, demonstrated by the inset autocorrelation function which was calculated considering the centres of the molecules as points. In the autocorrelation function, the rhombohedral lattice has the following (labelled) vectors: $a = 1.26 \pm 0.08$ nm, $b = 1.28 \pm 0.05$ nm.

Successive STM images of the same area indicate that Pn molecules diffuse at room temperature – both rotating and hopping across the surface. The mobility of the molecules is inferred in the streak–like tip artefacts in Figure 2(a). However, we find relatively stable positions by analysing the orientational anisotropy of the Pn molecules. Figure 2(b) shows a histogram of the molecular orientations. The angles are measured with respect to the absolute vertical direction of the image, $[01\bar{1}]$, which is marked with an arrow on Figure 2(a). The angles are shifted by $\sim$-7° for clarity, which is explained later. The purple bars represent the total distribution as calculated over 10 successive images, whilst the yellow bars show the orientations of molecules which are observed diffusing. It is clear, by both the total count and the ratio of diffusing to stationary molecules, that the most stable adsorption sites are those producing Pn orientations roughly perpendicular to the row direction of the substrate (0°). Conversely, the perpendicular 2–fold orientation (90°) is relatively unstable, a large proportion of these molecules actively diffusing.

By marking all molecules aligned along the $[01\bar{1}]$ direction, we find that they occupy two triangular sublattices which, together, form a honeycomb structure. Examples are indicated on Figure 2(a) with red/blue circles and black hexagons. A fully occupied unit cell of the red

distribution is also marked, with $c = 2.23 \pm 0.06$ nm, $d = 2.35 \pm 0.07$ nm i.e. twice the size of the lattice measured from the inset autocorrelation function. Notably, the third triangular lattice – whose inclusion into the red/blue honeycomb structure would recreate the lattice measured in the autocorrelation function – is unoccupied across the surface. Examples of these sites are highlighted by yellow circles at the centre of the hexagons.

The sublattice/honeycomb structure of the red/blue sites matches the distribution of small Tb triangles at the surface. This relationship is indicated in Figure 2(c) which shows a section of the model Tb atoms at the surface[22]. Two small triangles at the bottom are enclosed by blue and red circles, which are each distributed on rhombohedral lattices of $c = d = 2.09$ nm across the surface. These triangles are canted ~7° with respect to the $[01\bar{1}]$ direction and can also be linked by a black hexagon, with the centres of the triangles marked with either red or blue dots. The centre of the hexagon shows a yellow dot at the centre of a larger, subsurface Tb triangle and a dashed lined indicates the cell formed between red, blue, and yellow dots.

We can therefore speculate on potential adsorption sites for all orientations across the surface considering the match between the underlying Tb structure and the $[01\bar{1}]$–oriented molecule distribution. Figure 3 shows a collection of enlarged images from Figure 2(a) and model representations of Pn adsorption sites, dependent on orientation. Only orientations with significant peaks in Figure 2(b) are considered: 0°, 45°, 60° and 90° (including any mirror–equivalents) i.e. those commensurate with 2–fold row (0°, 45°, 90°) and 3–fold triangular (0°, 60°) symmetry. As previously mentioned, the Pn molecules are typically canted from these absolute orientations, roughly by the same small angle as the Tb triangles (7° with respect to the absolute vertical direction). For simplicity however, we label the figures with respect to the shifted histogram values.

From a geometric standpoint, each adsorption site involves Tb atoms interacting with the ends of the Pn molecule through either a) an on–top acene ring–Tb atom interaction (e.g. 45°), b) mirror symmetric pinning between two Tb atoms, presumably mediated by the H atoms on the acene ring (e.g. 90°), or c), a mixture of both. This observation is consistent with previous work of Pn adsorption on Tsai–type surfaces, where the molecules preferentially adsorb at the sparsely distributed rare earth atom positions[26,27]. Similarly, the relative chemical order of the Tb positions compared to the Au/Al atoms likely makes a more consistent 'choice' for the molecules.

Electronically, the signal observed by STM for the molecules generally show a double–lobe structure consistent with relatively poor molecular resolution of Pn on metal surfaces[28–30]. On a local level, the Pn molecules often exhibit a difference in contrast between the two lobes, demonstrated by the examples in 4(a). With STM, these differences can be considered as either a change in height, electronic contribution, or both. Analysis of the substrate under the brighter lobes indicates no change in morphology to cause a significant height modulation – despite the row structure of the reconstruction. Likewise, the length of the molecules in all orientations is equal, indicating a planar adsorption scheme independent of orientation. Therefore, we suggest that this effect is electronic.

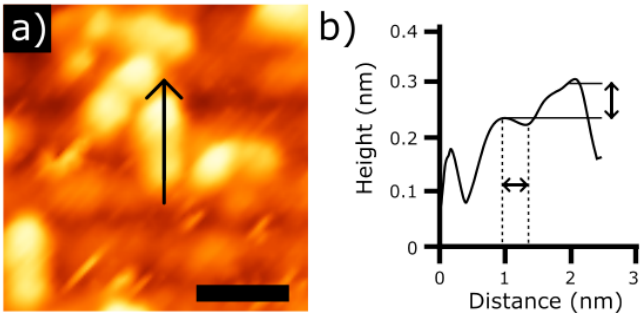

FIG. 4: ((**a**) STM image showing molecules with bright and dim lobes. An arrow indicates the direction of the line profile in **(b)**. Scale bar is 2 nm. **(b)** Line profile from **(a)**. Horizontal dashed lines indicate the distance between the dim lobe and the molecular centre. Solid horizontal lines mark the apparent lobe height difference.

To illustrate this, Figure 4(b) shows a line profile taken in the direction of the arrow marked in Figure 4(a). The profile indicates the apparent change in height along a 0° oriented molecule, marked by the two horizontal black lines, which on average across the image is measured as 0.05 ± 0.02 nm (for 0° molecules). For context, the apparent average height of all molecules above the substrate is ~0.8–1.2 nm, consistent with Pn on metal surfaces[28]. Furthermore, it appears that the brighter lobe is smeared towards the dimmer lobe, shifting the centre (or dip) of the molecular signal. This is demonstrated in Figure 4(b) by the dashed vertical lines, as measured from the dimmer lobe to the 'lowest' point in the molecule. Across the image for the 0° molecules, this distance is measured as 0.37 ± 0.06 nm, indicating an anisotropy in the electronic signal as the expected centre should be half of the electronic Pn length (~ 0.5 nm[28]). Measuring the height change and lobe–centre over all orientations shows that only the 0° molecules have one lobe which is consistently brighter and smeared towards the centre (i.e. the bright–lobe effect appears to cancel out over the other orientations).

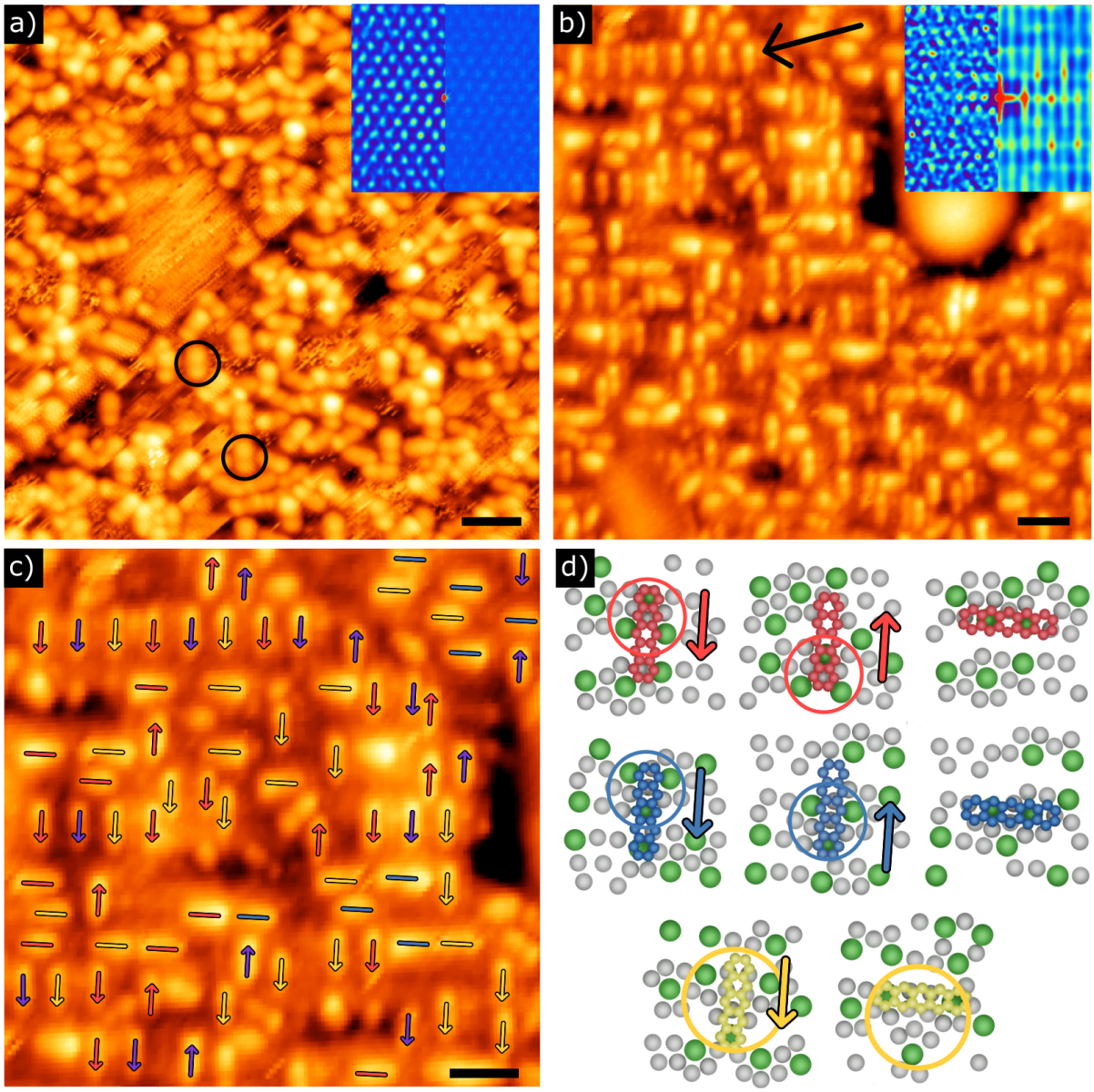

FIG. 5: **(a)** STM image (V_b = -1800 mV, I_t = 300 pA) of 0.7 ML of Pn with no post–annealing. Examples of molecules aligned along the vertical direction are marked by black circles. Inset (left) the autocorrelation function of the molecular centres. Inset (right) the autocorrelation function including the molecular orientations. Scale bar is 3 nm. **(b)** STM image (V_b = -1800 mV, I_t = 300 pA) of the same dose of Pn, after annealing to 600 K. The molecules show a clear preference for the vertical direction. A row of Pn molecules is highlighted by an arrow. Scale bar is 3 nm. **(c)** Individual Pn molecules are labelled with coloured arrows with respect to their adsorption sites. Red, blue, and yellow correspond to the Tb triangles in Figure 2(c). The direction of the arrow corresponds to the adsorption site geometry. A black–bordered white bar shows an anomalous position. Scale bar is 2 nm. **(d)** Model representation of the adsorption sites. The up and down arrows correspond to the positions of the molecules with respect to the Tb triangles. The coloured circles indicate the Tb triangles as in Figure 2(c).

Referring back to Figure 3, we see for the 0° molecules that the 'top' poles of both molecules lie in close proximity to 3 Tb atoms, while their 'bottom' poles are near 1–2. Meanwhile, the other orientations have (on average) equal local environments through their mirror–symmetric pairs. Therefore, we suggest that bright lobe effect is caused by the higher density of Tb atoms at the 0° sites, indicating a higher flow of electrons into these Pn poles. Indeed, the anisotropic smearing of the brighter lobes can be explained by the Tb triangles at the 0° sites in Fig-

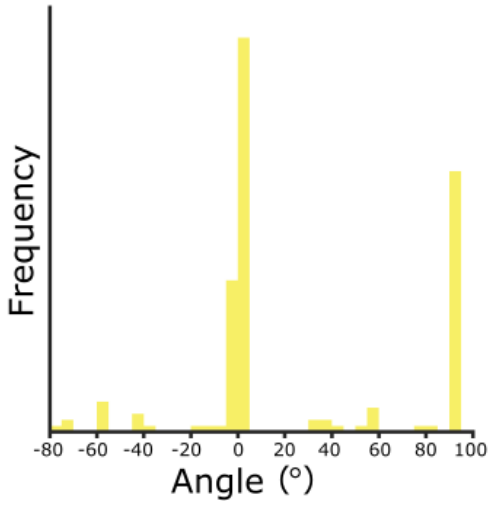

FIG. 6: Histogram of molecular orientation after post–deposition annealing to 600K. Compared to Figure 2(b), the range of molecular orientations has been reduced so that only vertical or horizontal molecules are observed.

ure 3(a) covering an area approximately equal to 3 acene rings out of 5. This would shift the apparent 'centre' of the molecule to the 2:3 ring junction or ∼ 0.4 nm from the bottom pole – an excellent match with the measured apparent centres.

We can speculate on the relative stability of the 0° site by directly comparing it to the other orientations in Figures 3(a–e). For the 90° site, both adsorption sites are commensurate with the row structure of the Au/Al atoms i.e., adsorbing along the troughs between adjacent rows. However, Figure 3(b) shows that the 90° positions are reliant on the Tb–pinning sites only. This suggests that the on–top acene ring interaction is a key to stability. Figures 3(c, e), orientations 45° and 60°, all show some degree of on–top acene ring–Tb interaction, however, they are also incommensurate with the 2–fold symmetry of the Au/Al row structure i.e., not in registry with the symmetric directions of the underlying surface. Figure 3(d), 60°, is a unique case, only appearing once within Figure 2(a). Indeed, it neither features on–top interaction, or symmetry sharing with the row–structure.

Figure 5(a) shows an STM image after further deposition of Pn molecules, approximately 0.7 ML, which was not post–annealed. Inset shows two auto–correlation functions with the same scale: the left is a function calculated from the centre positions of the molecules while disregarding their orientation, while the right considers both. It is clear that while the film is structurally ordered, the orientational structure of the molecules is relatively disordered. Figure 5(b) shows an STM scan after post–annealing the sample to 600 K. Inset left of Figure 5(b) shows an auto–correlation function of the molecular distribution independent of orientation, while inset right considers the orientation. A clear enhancement of a rectangular–like structure is observed. Likewise, the coverage is reduced, ∼ 0.5 ML, where Pn molecules which are not strongly bonded to the surface are presumed to desorb in the annealing process.

Figure 6 shows the histogram of molecular orientations after the annealing process, which reflects a clearer orthogonal preference in comparison to Figure 2(b). Now, the majority of molecules are aligned along the $[01\bar{1}]$ direction (∼56%), with several rows of linearised molecules observed, marked by an arrow in Figure 5(b). A minority of the Pn molecules are oriented 90° (∼27%), while the remaining ∼11% are either 60° or 45°. In comparison, the ratio of orientations in Figure 2(b) is ∼21% for 0°, ∼12% for 90°, with the remaining molecules orientated between 45°–60°.

Analysis of the Pn row structures indicate that the post–deposition annealing promotes new adsorption sites. Figure 5(c) shows an enlarged section of Figure 5(b), where the Pn molecules are now decorated with coloured arrows or bars. The colours represent the positions of the Tb triangles at the surface indicated in Figure 2(c), while the direction of the arrows indicate their relationship to these sites, explained in Figure 5(d). Here, the original 0° sites discussed in Figure 2(a) correspond to the red or blue down pointing arrows. The up arrows represent molecules adsorbed at the same Tb triangles which are now slightly shifted vertically with respect to the underlying substrate: red or blue circles indicate the respective Tb triangles at the surface. Yellow arrow sites involve the larger sub–surface Tb triangle, and only appear in one 'orientation' i.e. a down arrow. This is likely due to the large Tb triangle only appearing in one orientation at the surface, unlike the small triangles.

Horizontal (90°) Pn molecules are represented by coloured bars, and now appear to adsorb directly on top of the Au/Al rows (interpreted by the relative positions of the other molecules), unlike those in Figure 3(b). It is likely that the additional thermal energy allows the 90°–oriented molecules to escape the hollows between adjacent bright rows. For all of the horizontal molecules, two rings of the Pn molecule sit on–top of Tb atoms, either towards the centre (red/blue) or at the ends of the Pn (yellow).

IV. CONCLUSIONS

We have shown that Pn molecules deposited onto the (111) surface of the 1/1 Au–Al–Tb approximant form a rotationally aligned film after annealing to 370 K, influenced by the underlying 2–fold symmetry of the Au/Al row structure. Stable sites were found to involve rare–earth atoms either by an on–top Tb–acene ring in-

teraction, or by a pinning of the ring between two closely separated Tb atoms. Analysis of the apparent height difference and centre–points of the 0° molecule lobes indicated a greater electronic contribution at Tb–dense sites. Further deposition without annealing showed that the Pn molecules form a structurally ordered film with poor rotational order. Additional annealing to 600 K decreased the Pn coverage and promoted diffusion of the molecules, leading to a more strongly ordered film.

ACKNOWLEDGEMENTS

This work was supported by a Kakenhi Grant-in-Aid (No. 19H05817, 19H05818) from the Japan Society for the Promotion of Science (JSPS).

[1] K. Deguchi, M. Nakayama, S. Matsukawa, K. Imura, K. Tanaka, T. Ishimasa, and N. K. Sato. Crystal structure of superconducting 1/1 cubic Au–Ge–Yb approximant with Tsai-type cluster. *Journal of the Physical Society of Japan*, 84(1):015002, 2015.

[2] K. Deguchi, M. Nakayama, S. Matsukawa, K. Imura, K. Tanaka, T. Ishimasa, and N. K. Sato. Superconductivity of Au–Ge–Yb approximants with Tsai-type clusters. *Journal of the Physical Society of Japan*, 84(2):023705, 2015.

[3] T. Watanuki, S. Kashimoto, D. Kawana, T. Yamazaki, A. Machida, Yukinori Tanaka, and Taku J. S. Intermediate-valence icosahedral Au-Al-Yb quasicrystal. *Phys. Rev. B*, 86(9):094201, 2012.

[4] K. Deguchi, S. Matsukawa, N. K. Sato, T. Hattori, K. Ishida, H. Takakura, and T. Ishimasa. Quantum critical state in a magnetic quasicrystal. *Nat. Mat.*, 11(12):1013–1016, 2012.

[5] S. Jazbec, S. Vrtnik, Z. Jagličić, S. Kashimoto, J. Ivkov, P. Popčević, A. Smontara, H. J. Kim, J. G. Kim, and J. Dolinšek. Electronic density of states and metastability of icosahedral Au–Al–Yb quasicrystal. *Journal of Alloys and Compounds*, 586:343–348, 2014.

[6] K. Kamiya, T. Takeuchi, N. Kabeya, N. Wada, T. Ishimasa, A. Ochiai, K. Deguchi, K. Imura, and N. K. Sato. Discovery of superconductivity in quasicrystal. *Nat. Commun.*, 9(1):1–8, 2018.

[7] A. Ishikawa, T. Hiroto, K. Tokiwa, T. Fujii, and R. Tamura. Composition-driven spin glass to ferromagnetic transition in the quasicrystal approximant Au-Al-Gd. *Phys. Rev. B*, 93(2):024416, 2016.

[8] A. Ishikawa, T. Fujii, T. Takeuchi, T. Yamada, Y. Matsushita, and R. Tamura. Antiferromagnetic order is possible in ternary quasicrystal approximants. *Phys. Rev. B*, 98(22):220403, 2018.

[9] S Yoshida, S Suzuki, T Yamada, T Fujii, A Ishikawa, and R Tamura. Antiferromagnetic order survives in the higher-order quasicrystal approximant. *Phys. Rev. B*, 100(18):180409, 2019.

[10] H. Miyazaki, T. Sugimoto, K. Morita, and T. Tohyama. Magnetic orders induced by RKKY interaction in Tsai-type quasicrystalline approximant Au-Al-Gd. *Phys. Rev. Mater.*, 4(2):024417, 2020.

[11] T. J. Sato, A. Ishikawa, A. Sakurai, M. Hattori, M. Avdeev, and R. Tamura. Whirling spin order in the quasicrystal approximant Au72 Al14 Tb14. *Phys. Rev. B*, 100(5):054417, 2019.

[12] R. Tamura, Y. Muro, T. Hiroto, K. Nishimoto, and T. Takabatake. Long-range magnetic order in the quasicrystalline approximant cd 6 tb. *Phys. Rev. B*, 82(22):220201, 2010.

[13] H. Takakura, C. P. Gómez, A. Yamamoto, M. de Boissieu, and A. P. Tsai. Atomic structure of the binary icosahedral Yb–Cd quasicrystal. *Nat. Mater.*, 6(1):58, 2007.

[14] A. P. Tsai, J. Q. Guo, E. Abe, H. Takakura, and T. J. Sato. Alloys: A stable binary quasicrystal. *Nature*, 408(6812):537, 2000.

[15] A. P. Tsai. Icosahedral clusters, icosahedral order and stability of quasicrystals—a view of metallurgy. *Science and Technology of Advanced Materials*, 9(1):013008, 2008.

[16] J. K. Parle, A. Beni, V. R. Dhanak, J. A. Smerdon, P. Schmutz, M. Wardé, M-G. Barthés-Labrousse, B. Bauer, P. Gille, and H. R. Sharma. STM and XPS investigation of the oxidation of the Al4 (Cr, Fe) quasicrystal approximant. *Applied Surface Science*, 283:276–282, 2013.

[17] J. Ledieu, É. Gaudry, L. N. S. Loli, S. A. Villaseca, M-C. De Weerd, M. Hahne, P. Gille, Y. Grin, J-M. Dubois, and V. Fournée. Structural investigation of the (010) surface of the Al_{13} Fe_4 catalyst. *Phys. Rev. Lett.*, 110(7):076102, 2013.

[18] C. Chatelier, Y. Garreau, A. Vlad, J. Ledieu, A. Resta, V. Fournée, M-C. De Weerd, A. Coati, and É. Gaudry. Pseudo-2-Fold Surface of the $Al_{13}Co_4$ Catalyst: Structure, Stability, and Hydrogen Adsorption. *ACS Applied Materials & Interfaces*, 12(35):39787–39797, 2020.

[19] J. Ledieu, É. Gaudry, K. Pussi, T. Jarrin, P. Scheid, P. Gille, and V. Fournée. Reconstruction of the Al13Ru4 (010) approximant surface leading to anisotropic molecular adsorption. *The Journal of Physical Chemistry C*, 121(40):22067–22072, 2017.

[20] V. Fournée, A. R. Ross, T. A. Lograsso, J. W. Evans, and P. A. Thiel. Growth of Ag thin films on complex surfaces of quasicrystals and approximant phases. *Surface Science*, 537(1-3):5–26, 2003.

[21] V. Fournée, J. A. Barrow, M. Shimoda, A. R. Ross, T. A. Lograsso, P. A. Thiel, and A. P. Tsai. Palladium clusters formed on the complex pseudo-10-fold surface of the ξ'-Al77. 5Pd19Mn3. 5 approximant crystal. *Surface Science*, 541(1-3):147–159, 2003.

[22] S. Coates, K. Nozawa, M. Fukami, K. Inagaki, M. Shimoda, R. McGrath, H. R. Sharma, and R. Tamura. Atomic structure of the (111) surface of the antiferromagnetic 1/1 au-al-tb approximant. *Phys. Rev. B*, 102(23):235419, 2020.

[23] S. Hars, H. Sharma, J. Smerdon, T. Yadav, R. Tamura, M. Shimoda, and R. McGrath. The structure of the (100) surface of Ag-In-Gd 1/1 approximant. *Acta Physica Polonica A*, 126(2):479–481, 2014.

[24] S. S. Hars, H. R. Sharma, J. A. Smerdon, T. P. Yadav, A. Al-Mahboob, J. Ledieu, V. Fournée, R. Tamura, and R. McGrath. Surface structure of the Ag-In-(rare earth) complex intermetallics. *Phys. Rev. B*, 93(20):205428, 2016.

[25] R. Ruiz, D. Choudhary, B. Nickel, T. Toccoli, K-C. Chang, A. C. Mayer, P. Clancy, J. M. Blakely, R. L. Headrick, S. Iannotta, et al. Pentacene thin film growth. *Chemistry of Materials*, 16(23):4497–4508, 2004.

[26] J. A. Smerdon, K. M. Young, M. Lowe, S. S. Hars, T. P. Yadav, D. Hesp, V. R. Dhanak, A. P. Tsai, H. R. Sharma, and R. McGrath. Templated quasicrystalline molecular ordering. *Nano Lett.*, 14(3):1184–1189, 2014.

[27] A. Alofi, D. Burnie, S. Coates, R. McGrath, and H. R. Sharma. Adsorption of pentacene on the 2–fold surface of the icosahedral ag–in–yb quasicrystal. *Materials Transactions*, 62(3):312–316, 2021.

[28] J. Lagoute, K. Kanisawa, and S.n Fölsch. Manipulation and adsorption-site mapping of single pentacene molecules on cu (111). *Phys. Rev. B*, 70(24):245415, 2004.

[29] C. B. France, P. G. Schroeder, J. C. Forsythe, and B. A. Parkinson. Scanning tunneling microscopy study of the coverage-dependent structures of pentacene on au (111). *Langmuir*, 19(4):1274–1281, 2003.

[30] P. G. Schroeder, C. B. France, J. B. Park, and B. A. Parkinson. Energy level alignment and two-dimensional structure of pentacene on au (111) surfaces. *Journal of Applied Physics*, 91(5):3010–3014, 2002.